

Screening magnetic fields by superconductors: A simple model

Original

Screening magnetic fields by superconductors: A simple model / Caputo, J. G.; Gozzelino, Laura; Laviano, Francesco; Ghigo, Gianluca; Gerbaldo, Roberto; Noudem, J.; Thimont, Y.; Bernstein, P.. - In: JOURNAL OF APPLIED PHYSICS. - ISSN 0021-8979. - STAMPA. - 114:(2013), pp. 233913-1-233913-9. [10.1063/1.4848015]

Availability:

This version is available at: 11583/2524916 since:

Publisher:

AIP Publishing LLC

Published

DOI:10.1063/1.4848015

Terms of use:

This article is made available under terms and conditions as specified in the corresponding bibliographic description in the repository

Publisher copyright

(Article begins on next page)

Screening magnetic fields by superconductors: A simple model

J.-G. Caputo, L. Gozzelino, F. Laviano, G. Ghigo, R. Gerbaldo, J. Noudem, Y. Thimont, and P. Bernstein

Citation: [Journal of Applied Physics](#) **114**, 233913 (2013); doi: 10.1063/1.4848015

View online: <http://dx.doi.org/10.1063/1.4848015>

View Table of Contents: <http://scitation.aip.org/content/aip/journal/jap/114/23?ver=pdfcov>

Published by the [AIP Publishing](#)

Articles you may be interested in

[The universality of the magnetization irreversibility line of metglasses and superconductors](#)

Low Temp. Phys. **40**, 859 (2014); 10.1063/1.4897012

[Andreev reflection study of the new magnetic superconductor Mo₃Sb₇ in magnetic field](#)

Low Temp. Phys. **33**, 1009 (2007); 10.1063/1.2747078

[Spin screening of magnetic moments and inverse proximity effect in ferromagnet/superconductor nanostructures](#)

J. Appl. Phys. **99**, 08M506 (2006); 10.1063/1.2172910

[Penetration of ac magnetic field into bulk high-temperature superconductors: Experiment and simulation](#)

J. Appl. Phys. **95**, 6693 (2004); 10.1063/1.1667423

[Structural, Transport and Magnetic Properties of the Doped Magnetic Superconductor Ru-1212](#)

AIP Conf. Proc. **678**, 333 (2003); 10.1063/1.1612401

A promotional banner for the Journal of Applied Physics. It features the AIP logo and the journal title at the top. Below this, the text 'Meet The New Deputy Editors' is centered. At the bottom, there are three circular headshots of the new deputy editors, each with their name written to the right: Christian Brosseau, Laurie McNeil, and Simon Phillpot.

AIP | Journal of Applied Physics

Meet The New Deputy Editors

 **Christian Brosseau**

 **Laurie McNeil**

 **Simon Phillpot**

Screening magnetic fields by superconductors: A simple model

J.-G. Caputo,^{1,a)} L. Gozzelino,² F. Laviano,² G. Ghigo,² R. Gerbaldo,² J. Noudem,³ Y. Thimont,³ and P. Bernstein³

¹*Laboratoire de Mathématiques, INSA de Rouen, Avenue de l'Université, 76801 Saint-Etienne du Rouvray, France*

²*Department of Applied Science and Technology, Politecnico di Torino, 10129, Torino, Italy*

³*CRISMAT/LUSAC, Physics Department, Université de Caen, France*

(Received 5 August 2013; accepted 30 November 2013; published online 20 December 2013)

We introduce a simple approach to evaluate the magnetic field distribution around superconducting samples, based on the London equations; the elementary variable is the vector potential. This procedure has no adjustable parameters, only the sample geometry and the London length, λ , determine the solution. This approach was validated by comparing the induction field calculated to the one measured above MgB₂ disks of different diameters, at 20 K and for applied fields lower than 0.4 T. The model can be applied if the flux line penetration inside the sample can be neglected when calculating the induction field distribution outside the superconductor. We conclude by showing on a cup-shape geometry how one can design a magnetic shield satisfying a specific constraint. © 2013 AIP Publishing LLC. [<http://dx.doi.org/10.1063/1.4848015>]

I. INTRODUCTION

Magnetic field screening is very important for a large variety of applications. Very low magnetic field background are required when high resolution magnetic field detector are used (e.g., SQUID^{1,2}). Magnetic shielding is also used to solve problems of electromagnetic compatibility among different devices, i.e., to allow the simultaneous use of multiple diagnostic devices, including the magnetic resonance imaging.³ Finally, let us mention military applications.⁴

Depending on the application, active⁵ or passive^{6,7} shielding solutions can be adopted. In the static or quasi-static regimes passive shielding can be achieved using ferromagnetic and/or superconducting materials. The former, but not the latter, can operate at room temperature. However, the latter, due to the Meissner effect, show the highest shielding efficiency.

For type-II superconductors, complete magnetic shielding occurs only when the total field is below the value of the lower critical field, B_{c1} . Here, we disregard the surface region of depth λ , the London penetration depth, where shielding currents are confined. If the applied field is much larger than B_{c1} , a description of the magnetic field of the superconductor cannot disregard the penetration of vortices and their movement inside the material. Several experiments of magnetic shielding have been carried out in the last years, using both low-Tc and high-Tc superconducting materials operating in the mixed state. In this state, the interpretation of the experimental results requires to calculate the flux lines distribution inside and outside the sample. One needs models such as the critical state model^{8–10} associated with a constitutive law giving the non-linear dependence of the electric field on the current density to account for the energy dissipation due to vortex motion.^{7,11,12} Because of this complexity, this approach yields exact solution only in few idealized cases.¹³

In addition to the material, the geometry of the shield is an important issue. Some applications require to design magnetic shields with complex geometries. Moreover, an approach to calculate easily how the shield geometry influences the field distribution outside the sample is the first step towards solving the inverse problem of designing a magnetic shield starting from given requirements.

Aiming at this, we introduce an approach based on the London equations, where the elementary variable is the vector potential A .^{14,15} The order parameter is assumed constant throughout the sample leading to a very simple London equation for A . There the medium is represented by a source term. This formulation guarantees the continuity of the vector potential and gives in a simple way the magnetic induction field everywhere. In particular, it allows us to study in detail the field outside the sample and to take into account easily the demagnetization field. This model is strictly valid only for applied fields below B_{c1} . However, it is possible to extend its application to magnetic fields larger than the lower critical one, provided that the vortex penetration inside the sample does not change much the magnetic field distribution outside the sample itself. This holds if the magnetic field amplitude outside the sample scales linearly with the applied field as expected from our theory. Note that this London approach is a reduction of the more complex Ginzburg-Landau theory whose numerical solution was applied to superconducting meso-scale samples of different topologies^{16–18} to study the vortices inside the samples^{16,17,19} and the field distribution outside.¹⁷

Our London approach was validated by comparing the calculated solution with the experimental measures on three MgB₂ disks with different aspect ratio. The numerical results agree quantitatively with the measures for applied fields lower than 0.4 T. We chose this superconducting material because of its numerous advantages. First of all, its working temperature (10–30 K (Ref. 20)) can be easily reached using one-stage cryogen free cryocoolers. Then this material shows

^{a)}E-mail: caputo@insa-rouen.fr

higher B_{c1} and coherence length, ξ , than high-Tc cuprates. This last property ensures the transparency of grain boundaries to current flow.²¹ The important consequences are that one can work with polycrystalline samples and one can produce specimens with complex shapes assembled by soldering elementary pieces.^{22,23} Finally, the low density value of MgB_2 makes this material a good candidate for applications where weight constraints are present.

The article is organized as follows. In Sec. II, we derive the model from first principles and show how it is solved. Section III describes the fabrication of the samples and the experimental details of the characterization. The experimental data are presented and discussed in comparison with the model predictions in Sec. IV. Section V shows how a practical magnetic screen can be designed based on a quantitative criterion.

II. THE MODEL

The Maxwell equations of magnetostatics are

$$\nabla \cdot \mathbf{B} = 0, \quad \nabla \times \mathbf{B} = \mu_0 \mathbf{J}, \quad (1)$$

where \mathbf{B} is the magnetic induction field and \mathbf{J} is the current density. The electric field is omitted because we consider that the superconductor is only in the Meissner state. We introduce the vector potential \mathbf{A} such that

$$\mathbf{B} = \nabla \times \mathbf{A}.$$

Taking the curl of the second equation in (1), we get

$$-\nabla^2 \mathbf{A} = \mu_0 \mathbf{J}, \quad (2)$$

where we have assumed the London gauge

$$\nabla \cdot \mathbf{A} = 0.$$

The London hypothesis, i.e., there is no phase momentum in the superconductor¹⁵ implies

$$\mu_0 \mathbf{J} = -\frac{1}{\lambda^2} \mathbf{A}, \quad (3)$$

where λ is the London penetration depth. Combining Eqs. (2) and (3), we get

$$\nabla^2 \mathbf{A} = \frac{1}{\lambda^2} \mathbf{A}. \quad (4)$$

Note that the current \mathbf{J} only exists in the superconductor, outside it is zero. The equation can then be written so it describes the field everywhere inside and around the superconductor. It reads

$$\nabla^2 \mathbf{A} = \frac{1}{\lambda^2} \mathbf{A} I(\mathbf{r}), \quad (5)$$

where $I(\mathbf{r}) = 0$ (resp. $I(\mathbf{r}) = 1$) outside (resp. inside) the superconductor.

This equation is a first order description of the superconductor in the sense that we assumed the order parameter Ψ

to be spatially uniform, i.e., the superconductor is in the Meissner state. To see this consider the Ginzburg-Landau system of equations for \mathbf{A} and Ψ (Ref. 14)

$$\frac{1}{2m} \left(\frac{\hbar}{i} \nabla - 2e\mathbf{A} \right)^2 \Psi - \alpha \Psi + \beta \Psi |\Psi|^2 = 0, \quad (6)$$

$$\mathbf{J} = Im \left(\Psi^* \left(\frac{\hbar}{i} \nabla - 2e\mathbf{A} \right) \Psi \right), \quad (7)$$

where e is the charge of the electron and m its effective mass. We introduce the coherence length ξ , the equilibrium order parameter ψ_0^2 , and the London penetration depth λ as

$$\xi = \sqrt{\frac{\hbar^2}{2m\alpha}}, \quad \psi_0^2 = \frac{\alpha}{\beta}, \quad \lambda = \sqrt{\frac{m}{4\mu_0 e^2 \psi_0^2}}. \quad (8)$$

Substituting these quantities in the Ginzburg-Landau equations, we get

$$-\left(\nabla - i \frac{2e}{\hbar} \mathbf{A} \right)^2 \Psi - \frac{\Psi}{\xi^2} + \frac{4\mu_0 e^2 \lambda^2}{m \xi^2} \Psi |\Psi|^2 = 0. \quad (9)$$

The equation for the current becomes

$$\mathbf{J} = -\frac{1}{\mu_0} \frac{1}{\lambda^2} \mathbf{A} + \frac{2e\hbar}{m} Im(\Psi^* \nabla \Psi).$$

Collecting all the terms of \mathbf{J} and substituting into Maxwell's equation (2), we obtain the more general model

$$\Delta \mathbf{A} = \frac{\mathbf{A}}{\lambda^2} - \frac{2e\hbar}{m} Im(\Psi^* \nabla \Psi), \quad (10)$$

containing the vortex contribution. The comparison with the experiments presented below shows that (5) provides a good description of the fields around MgB_2 disks at 20 K and for applied fields below 0.4 T. For these type II superconductors where $\kappa = \lambda/\xi \gg 1$, the decay distance of the order parameter ξ is much smaller than the decay distance of the field, λ . Then the size of the vortices is small and the correction on the right hand side of (10) due to Ψ can be ignored in a first approximation.

In the experiment, we used disk-shaped MgB_2 samples placed on the axis of a solenoid producing a constant field B_0 as in Ref. 24. Therefore, in order to reproduce the experimental results, in the model, we assume a cylindrical symmetry for the magnetic field \mathbf{B} . Then the vector potential has only one component

$$\mathbf{A} = A \vec{\theta},$$

and is such that

$$\mathbf{B} = \nabla \times \mathbf{A} = -A_z \mathbf{r} + \frac{1}{r} (rA)_r \mathbf{z}, \quad (11)$$

where \mathbf{r} , \mathbf{z} are the unit vectors along the r and z directions, respectively, and the underscores represent partial

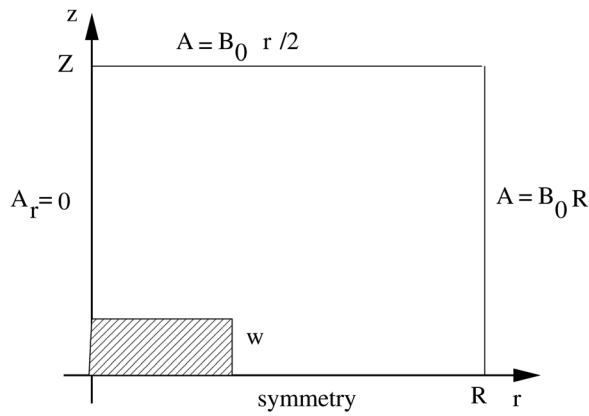


FIG. 1. Computational domain for the solution of Eq. (12) in the (r, z) plane. The boundary conditions are indicated.

derivatives. Since \mathbf{A} can be considered as a scalar, the Eq. (5) reduces to

$$\Delta A = \frac{1}{\lambda^2} I(r, z) A. \quad (12)$$

This equation for A needs to be integrated in the (r, z) plane. The computational domain is shown in Fig. 1 for the case of a disk of thickness $2w$, a sample that is symmetric with respect to the plane $z=0$. The boundary conditions are indicated on Fig. 1. For $r=0$, the magnetic field is along z so $A_z=0$. At a large distance from the sample, the field is assumed constant, equal to B_0 and parallel to z . The boundary condition is then $A = B_0 R/2$ where R is the edge of the solenoid generating the field. To summarize we have the following:

$$z = 0, \quad A \text{ symmetric}, \quad (13)$$

$$z = Z \gg 0, \quad A = \frac{B_0 r}{2}, \quad (14)$$

$$r = 0, \quad A_z = 0, \quad (15)$$

$$r = R, \quad A = \frac{B_0 R}{2}. \quad (16)$$

The only approximation is that we assume the field to be equal to B_0 for large $z=Z$. Typically, we took $Z=100w$ and made sure that the results do not depend on this value. Of course if the sample is not symmetric with respect to z , we need to consider the two boundaries $z = \pm Z$.

We present results obtained by solving Eq. (12) using the finite element software Comsol.²⁵ As stressed above, the problem is linear so that A can be scaled arbitrarily. Also the unit of length has been chosen as mm for commodity. Then the dimensions of the sample and the London penetration depth are all given in mm. The London penetration depth we have chosen at 20 K is $\lambda = 1.6 \times 10^{-4}$ mm. It is in the range of the measurements reported in Ref. 26. Concerning the boundary conditions in Fig. 1, we stress that the position of the boundary $z=Z=40$ is arbitrary. It corresponds to a value for which the screening field has decayed enough so that $B=B_0$. Fig. 2 presents a typical result of the magnetic field

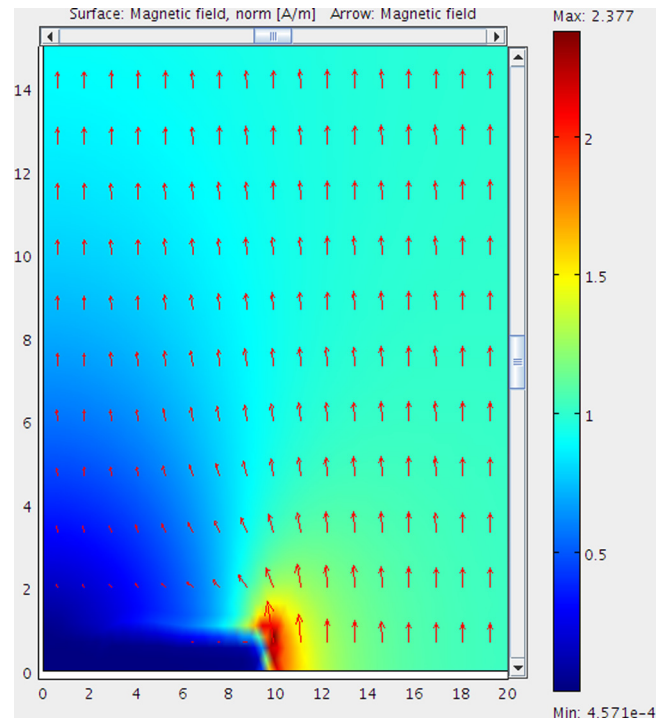


FIG. 2. Numerical integration of the Maxwell/London Eq. (12) for the disk D_1 showing B as a vector field and with $|B_0| = 1$.

B for an applied field $B_0=1$ for the disk geometry D_1 (see Table I below). Since the problem is linear, the magnitude of B_0 can be chosen arbitrarily. B ranges from 0 to 2.4 and is near zero in the superconductor. The curvature of the flux-lines outside the superconductor reduces the induction field near the upper surface of the superconductor. This effect is reinforced as the radius of the disks increases. Note the field reinforcement at the boundary $r=9.75$ mm of the disk. In fact the field at the interface is singular in this model because of the jump in ∇A .

This model allows to calculate the magnetic induction field distribution everywhere around a superconducting sample. It avoids the complications coming from the computation of the demagnetizing field. It can even be used when the external field is inhomogeneous. However, the main advantage of this model is the possibility to solve the inverse problem of designing a magnetic shield using as starting constraints the external applied field, the geometry of the shielded region and the tolerance for the field in that region. Of course this approach can be rigorously applied when the flux density penetration in the sample can be disregarded. However, for the large samples expected for shielding applications the initial vortex penetration at the surfaces will not change the outside field radically from the one calculated

TABLE I. Dimensions of the three disks analyzed.

Disk	Diameter (mm)	Thickness (mm)
D_1	19.5	1.90
D_2	14.8	1.75
D_3	8.1	1.80

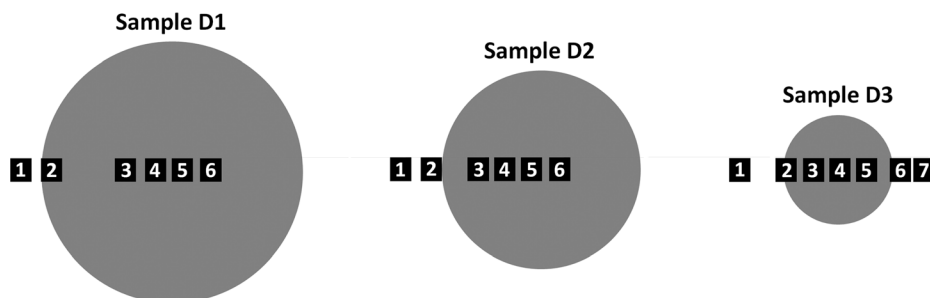


FIG. 3. Hall probe arrays for measuring the z component of the magnetic field for the three samples of Table I.

using our approach. This is due to geometric effects resulting from the Laplacian equation or, in other words, to the demagnetizing energy of the bulk Meissner state. We will come back to this point below.

III. SAMPLES FABRICATION AND CHARACTERIZATION TECHNIQUE

Three disk-shaped MgB_2 samples were fabricated by non-conventional Spark Plasma Sintering (SPS).²⁷ Their dimensions are reported in Table I. The samples were fabricated by pouring the commercially available MgB_2 powder²⁸ into a graphite mould, placed into the working chamber that was evacuated down to a pressure of 1 mbar. A pulsed electric current (2000 A, 4 V) was passed through the sample to raise the temperature up to 1200 °C in 7 min. The samples were kept at this temperature for 5 min under a 50 MPa uniaxial pressure. Finally, they were cooled down to room temperature in 8 min. The disks obtained were rectified by mirror polishing using pure ethanol as a lubricant. The relative density of the samples was more than 98% of the theoretical value, their Vickers hardness was 1050 MPa and their critical temperature was $T_c = 37$ K.

The measures were carried out at a temperature of 20 K in a uniform dc magnetic field up to 1.5 T. These fields were applied in the z direction, i.e., perpendicularly to the sample surface. They are generated by a superconducting cryogen free coil coaxial to the samples. The samples were mounted on the top of the second cooling stage of a cryocooler with an interposed 0.125 mm thick indium sheet to guarantee a good thermal contact and thus avoid thermo-magnetic instabilities causing flux jumps.^{29,30} These would strongly modify the shielding capability of the sample and, in the worst case, could create cracks and irreversible damage. A schematic view of the experimental set-up is reported in Ref. 31.

The z component of the magnetic induction, i.e., the component parallel to the applied magnetic field direction, was measured with a GaAs Hall probe array mounted on the bottom surface of a custom-designed motor-driven stage, able to be moved along the sample axis with a spatial resolution of 1 μm . Each probe has a disk-shaped active area with a diameter of 300 μm and an average sensitivity of 43.2 mV/T for a bias current of 0.1 mA. The probes were aligned along the sample diameter following the radial arrangement reported in Fig. 3. The radial positions are detailed in Table II for each sample.

The sample temperature, the applied magnetic field, the Hall probe positioning, and the Hall voltage were controlled with a LabviewTM custom program. The experiments were

TABLE II. Radial distance of the probes from the center for each sample. All the dimensions are in mm; the error in the position of each probe is about 0.2 mm.

Disk	Radius	d	d	d	d	d	d	d
D1	9.75	−11.2	−9.8	−3.2	−1.2	0.8	2.8	...
D2	7.40	−10.5	−8.2	−4.7	−2.7	−0.7	1.3	...
D3	4.05	−7.4	−3.9	−1.9	0.1	2.1	4.6	6.4

performed after a zero-field cooling. The magnetic field was gradually increased up to a predetermined value. The induction field profiles were recorded for different distances z above the sample.

IV. ANALYSIS OF THE EXPERIMENTAL DATA

An important consequence of the London approximation is that the model is linear so the results should scale with the magnetic field B_0 . We have tested this scaling on the experimental data for the three disks analyzed. The main result is that for all three samples the experimental curves scale as B/B_0 as long as $B_0 < 0.4$ T. The scaling is perfect up to 0.1 T and above that value there are small differences especially close to the center of the disk. It is worthwhile to remember that only the z component of the field B is measured.

We first show the results for a small applied field $B_0 < 0.1$ T. In Fig. 4, we present B/B_0 as a function of the distance z from the superconductor surface for $B_0 = 0.04$ T, 0.07 T, and 0.1 T at different radial positions for the three samples D_1 , D_2 , D_3 . In the following B/B_0 vs. z plots, the variable z is the distance above the superconductor. As expected there is a very good scaling. The shielding effect is maximum near the sample center and decreases towards the edges. Samples of large diameter screen the field better than the ones with a small diameter. The upper curvature of the field lines detected near the outer edge of the samples is due to the field reinforcement as we will show below. It was seen in the demagnetization field calculated by Brandt at the disk edges.⁹ It is more pronounced in the sample D_1 because it has the largest diameter.

When the applied field is increased up to 0.4 T, the scaling remains quite good even if some discrepancies start emerging. We show in Fig. 5 the ratio B/B_0 as a function of z for $B_0 = 0.1$ T, 0.2 T, and 0.4 T. Again the three panels correspond to the three samples. These results confirm that a linear theory such as the London equation can describe well the disk data for magnetic fields smaller than 0.4 T at 20 K.

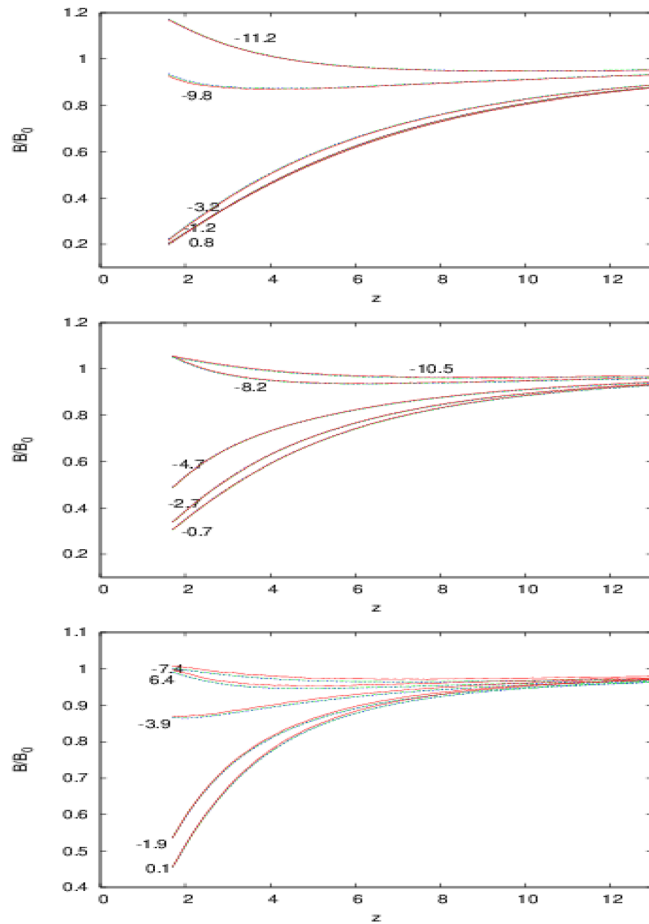


FIG. 4. Plot of B/B_0 as a function of the distance z above the superconductor for $B_0 = 0.04$ T (continuous line, red online), for $B_0 = 0.07$ T (long dashed line, green online), $B_0 = 0.1$ T (short dashed line, blue online), and for different radial positions. The three panels correspond to the three samples D_1, D_2, D_3 from top to bottom.

We now use these values of B_0 to compare the solution of the London Eq. (5) with the experimental data. The results are shown in Fig. 6 for the disk sample D_1 . There the experimental data are shown as lines for clarity. Only the value $B_0 = 0.1$ T is presented since we have a good scaling B/B_0 as shown previously. The agreement is reasonably good for all the radial positions. For the disks 2 and 3, we observe a similar trend as shown in Figs. 7 and 8.

When the field B_0 is increased, vortices penetrate the sample so that the phase cannot be considered as uniform. Then the vector potential A does not depend linearly on the applied field B_0 .

Fig. 9 presents the B/B_0 ratios for $B_0 = 0.4$ T, 0.8 T, and 1 T. For small radii the field B increases faster than B_0 so that the screening is not as efficient as for smaller B_0 . Vortices probably penetrate the sample and the model needs to be corrected to take them into account. Notice that the discrepancies are larger when one is closer to the center of the disks. On the edges the scaling is preserved. This can be understood by examining the numerical results. Fig. 10 shows the calculated \mathbf{B} in a region close to the samples for D_1 (top panel), D_2 (middle panel), and D_3 (bottom panel).

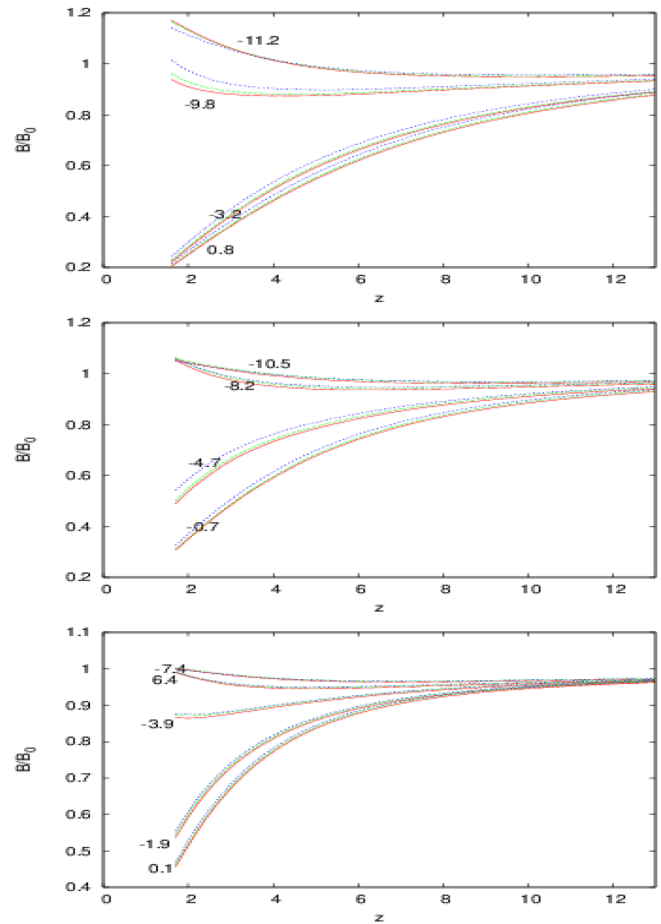


FIG. 5. Plot of B/B_0 as a function of the distance z above the superconductor for $B_0 = 0.1$ T (continuous line, red online), 0.2 T (long dashed line, green online), 0.4 T (short dashed line, blue online), and for different radial positions. The three panels correspond to the three samples D_1, D_2, D_3 from top to bottom.

The screening region where the field is close to zero is a triangle $z < R_1/2 - 0.3r$ for the sample D_1 , $z < R_2/2 - 0.43r$ for the sample D_2 , and $z < R_3/2 - 0.5r$ for the sample D_3 , where R_1, R_2 , and R_3 are the radii of the disks D_1, D_2 , and D_3 , respectively. The region screened by the disk D_1 is twice as large as the one screened by the disk D_3 . Note also

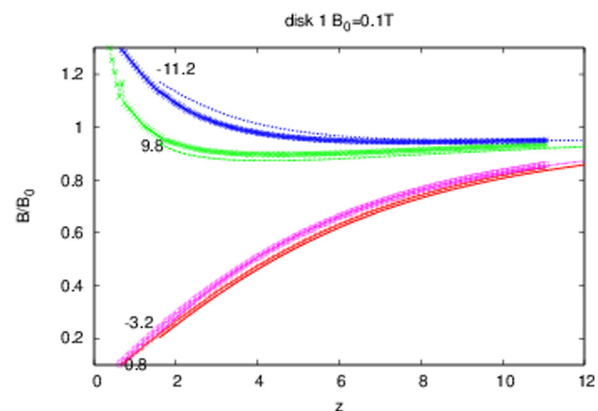


FIG. 6. Comparison between the ratio B/B_0 calculated and measured for sample D_1 as a function of the distance z above the superconductor and for different r . The measurement temperature was $T = 20$ K and $B_0 = 0.1$ T. The experimental data are shown with lines and the numerical values are plotted with symbols. The different values of r are reported in the figure.

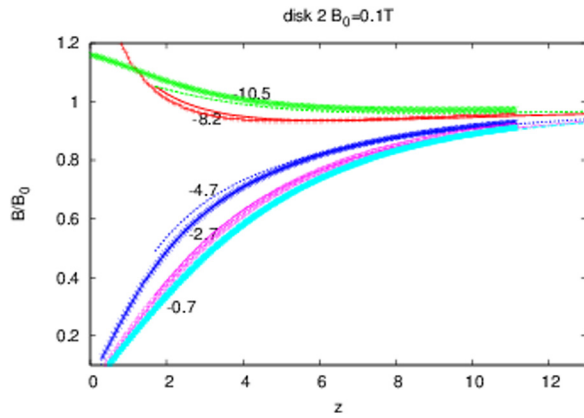


FIG. 7. Comparison between the ratio B/B_0 calculated and measured for sample D_2 as a function of the distance z above the superconductor and for different r . The other parameters are the same as in Fig. 6.

that the field reinforcement is 2.4 for the disk D_1 while it is 1.9 for the disk D_3 . The experimental data of Fig. 9 show that the scaling is partially preserved close to the outer edge of the disks. This is precisely where the model predicts a field reinforcement. Therefore, it seems that this reinforcement is maintained even when vortices are present. This needs to be confirmed by more detailed observations.

V. DISCUSSION AND CONCLUSION

From the results shown in Sec. IV, we see that the Maxwell/London model (5) is appropriate to describe in a simple way the magnetic induction field distribution outside disk-shaped MgB_2 samples at 20 K for applied fields lower than 0.4 T. From the model, it is easy to compute the shielding field, $\mathbf{B}-\mathbf{B}_0$, generated by the disks. We show this field in Fig. 11 with the arrows, while the modulus of the total field \mathbf{B} is shown with the color code. The superconductor induces a redistribution of the induction field around itself. In particular, notice the shielding effect above the upper surface of the sample where the superconductor generates a field that is exactly opposed to the applied field. There is also a strong field reinforcement right outside the disk, for $z=0$, $r > R_1$, where the shielding field is aligned with the applied field.

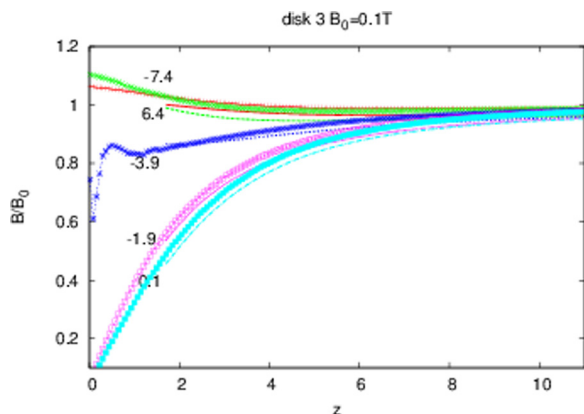


FIG. 8. Comparison between the ratio B/B_0 calculated and measured for sample D_3 as a function of the distance z above the superconductor and for different r . The other parameters are the same as in Fig. 6.

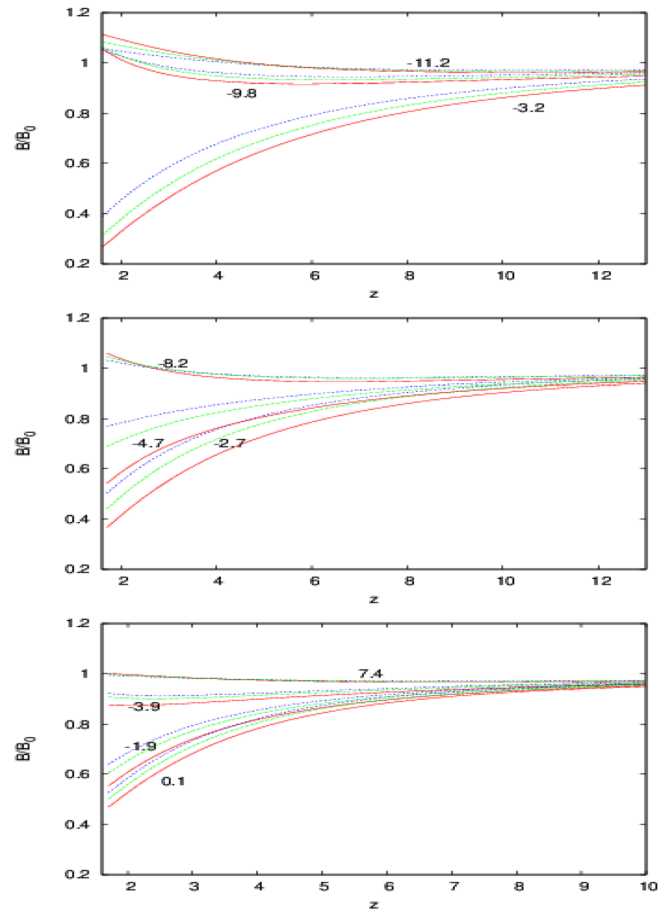


FIG. 9. Ratios B/B_0 as a function of the distance z above the superconductor for $B_0 = 0.4$ T (continuous line, red on line), 0.8 T (long dashed line, green on line), 1 T (short dashed line, blue on line), and different radial positions. The three panels correspond to the samples D_1 , D_2 , D_3 from top to bottom.

This magnetic flux distribution allows to design a magnetic screen. This design is a problem of shape optimization which is difficult to solve in general. A simplification is to assume that the shape depends on a parameter and to minimize a criterion with respect to this parameter. The study done on the disk guides us towards an ideal geometry. In particular, we want to avoid the regions where the field is reinforced and we want the screening field to remain aligned and opposite the applied field in the screening region. From our calculations and the results reported in the literature,¹¹ assuming a non-ideal system with a low height/radius aspect-ratio, a good candidate is a cup-shaped screen, see Fig. 12. This will also show that our method can be applied to superconductors of different shapes. Inside the cup, the screening field has a direction opposite to the applied field. For this geometry, a characteristic parameter is the height h . Then one would minimize the magnetic field \mathbf{B} in a given domain Ω with respect to h . One could also minimize the normalized magnetic energy in Ω ,

$$\mathcal{E} = \frac{1}{B_0^2} \int_{\Omega} \mathbf{B}^2 dr dz = \frac{1}{B_0^2} \int_{\Omega} dr dz \left[A_z^2 + \left(\frac{1}{r} (rA)_r \right)^2 \right]. \quad (17)$$

For the cup, the domain Ω will be a subset of the cup interior. We can fix Ω to be

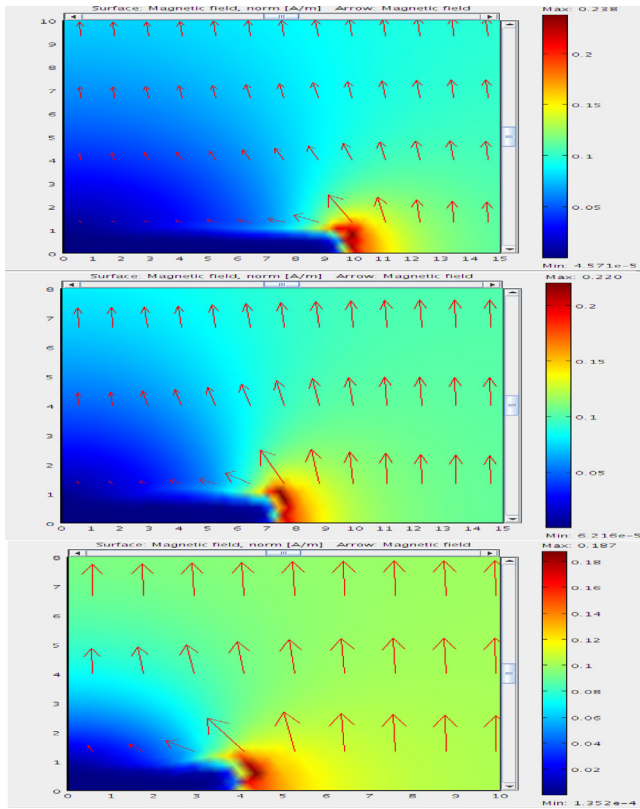


FIG. 10. Blow-up of the region close to the samples showing how screening is enabled. The magnetic induction field \mathbf{B} is shown with arrows and its magnitude is in the color code. The three samples are D_1 (top), D_2 (middle), and D_3 (bottom). The maximum of $|\mathbf{B}|$ in dark red (online) is 0.24 for D_1 , 0.22 for D_2 , and 0.19 for D_3 . The z range is $z < 10$ (top panel) and $z < 8$ (middle and bottom panels). The applied field is $B_0 = 0.1$.

$$\Omega = \{a \leq z \leq 1.5a, r \leq r_i\}. \quad (18)$$

We solve numerically (5) for the cup in a different way than for the disk because the cup does not have a mirror symmetry. Instead we apply the same boundary condition (14) at the two extremities $z = \pm Z$.

Let us now illustrate this quantitatively. We have chosen $a = 3$ mm, $r_i = 9$ mm, $r_e = r_i + a$. We then find the minimum h value so that the average induction field inside the domain Ω is below a tolerance value. Of course, for each

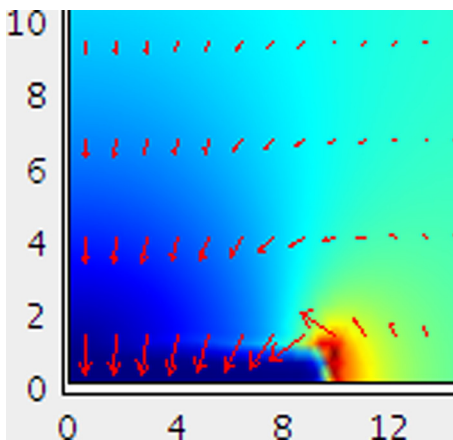


FIG. 11. Screening field $\mathbf{B} - \mathbf{B}_0$ of disk D_1 shown as arrows. The total field, \mathbf{B} , is shown with the color code as in Fig. 10.

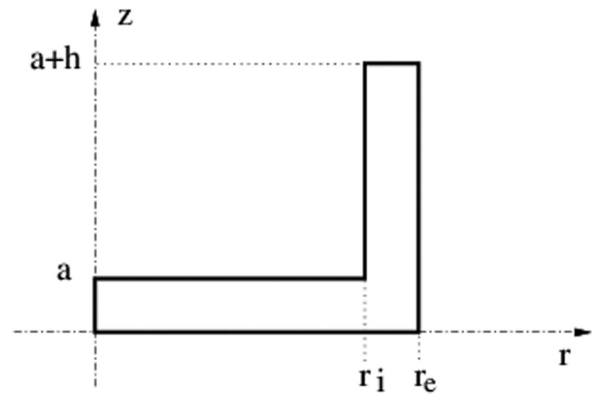


FIG. 12. Schematic drawing of a magnetic screen in the form of a cup of depth h .

volume chosen, there is only one minimum h value such that the average induction field is below a tolerance value. Higher h values are obviously acceptable. To show this we consider three different values of the cup depth $h = 2$ mm, 4 mm, and 8 mm. The sizes were chosen to demonstrate the feasibility of the object. They can be rescaled in order to meet other experimental constraints. We take $B_0 = 1$ so as not to scale the field in Eq. (17). Since the problem is linear, the unit of the field is arbitrary. Fig. 13 shows the magnetic field for a cup where $h = 4$ mm. The vector field \mathbf{B} is drawn and its modulus is given by the color code. Notice the strong reinforcement at each edge of the cup. The dark region (dark blue online) confirms that the field is very small in the interior of the cup.

As h is increased, the field is reduced inside the cavity. Fig. 14 shows the field in the cavity ($r \leq 9$ mm) for a given z

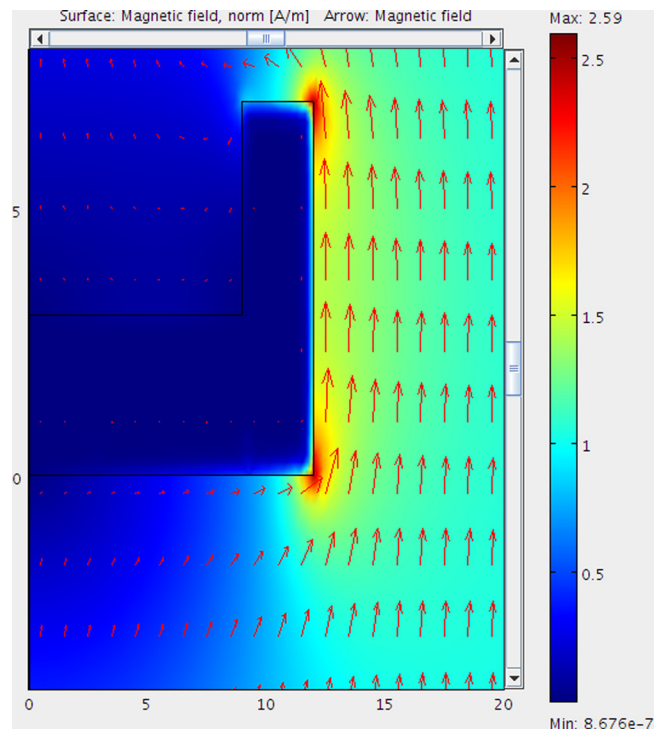


FIG. 13. Magnetic induction field direction (arrows) and modulus (in color code) for a cup shield.

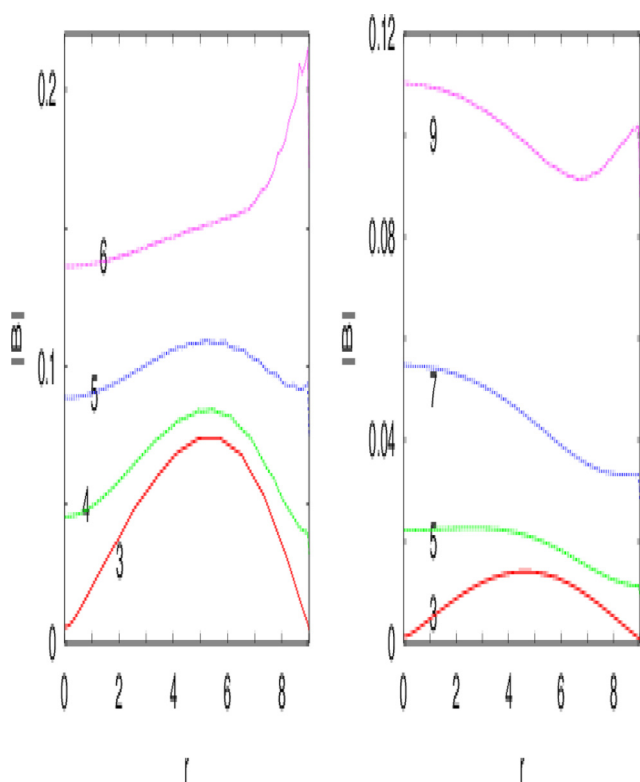


FIG. 14. Magnetic induction field modulus inside the cup as a function of r for different values of z . Two different cup depths are shown, $h = 4$ mm (left panel) and $h = 8$ mm (right panel). The values of z are indicated on the figures.

as a function of r . The left panel corresponds to $h = 4$ mm and $z = 3$ mm, 4 mm, 5 mm, and 6 mm while the right panel is for $h = 8$ mm and $z = 3$ mm, 5 mm, 7 mm, and 9 mm. We see that for $z < a + 2$ mm (2 mm above the bottom of the cup) and for $h = 4$ mm, we have

$$5\% \leq \frac{B}{B_0} \leq 10\%.$$

As expected, increasing the height of the cup reduces the field inside the cup. When $h = 8$ mm and $z < a + 4$ mm, we have

$$1\% \leq \frac{B}{B_0} \leq 5\%.$$

Therefore, increasing the cup depth, one can completely suppress the magnetic field to a given tolerance so that we can then realize a suitable screen.

In summary, we have shown that the Maxwell/London model is suitable to describe the magnetic field redistribution induced by a superconducting sample. This approach was validated by comparing the numerical solutions to the values of the induction field measured above disk-shaped MgB₂ samples. At $T = 20$ K, the agreement is good for external applied field lower than 0.4 T.

The study indicates that the model can be used also above the lower critical field, provided that the penetration of the flux lines inside the sample contributes weakly to the field values outside the superconductor itself. However, this

should be checked by comparing the numerical results with the experimental ones.

The model has no adjustable parameters, since the London penetration length is a characteristic of the superconducting material used in the experiment and is introduced a priori. This approach can be used for superconductors of whatever shape; it also applies when the external field is inhomogeneous.

Starting from these results, we demonstrated on a cup geometry, how to design an efficient magnetic field screen by minimizing the magnetic energy in a given region. This minimization is easy because the direct problem is so simple. The minimum cup height h is such that the average field inside a sub-region of the cup interior is below a given tolerance. This is a first step towards designing efficient magnetic field screens.

ACKNOWLEDGMENTS

J.G.C. thanks Michael Sigal for very helpful discussions. The authors are grateful to the Centre de Ressources Informatiques de Haute Normandie where most of the calculations were done. J.G.C. thanks the Department of Mathematics of the University of Arizona for its hospitality during a sabbatical visit.

- ¹H. Xia, A. B.-A. Baranga, D. Hoffman, and M. V. Romalis, *Appl. Phys. Lett.* **89**, 211104 (2006).
- ²R. Körber, A. Casey, A. Shibahara, M. Piscitelli, B. P. Cowan, C. P. Lusher, J. Saunders, D. Drung, and Th. Schurig, *Appl. Phys. Lett.* **91**, 142501 (2007).
- ³G. Delso and S. Ziegler, *Eur. J. Nucl. Med. Mol. Imaging* **36**, 86 (2009).
- ⁴O. Baltag, D. Costandache, M. Rau, A. Iftemie, and I. Rau, *Adv. Electr. Comput. Eng.* **10**, 135 (2010).
- ⁵R. Harrison, R. Bateman, J. Brown, F. Domptail, C. M. Friend, P. Ghoshal, C. King, A. Van der Linden, Z. Melhem, P. Noonan, A. Twin, M. Field, S. Hong, J. Parrell, and Y. Zhang, *IEEE Trans. Appl. Supercond.* **18**, 540 (2008).
- ⁶Y. Seki, D. Suzuki, K. Ogata, and K. Tsukada, *Appl. Phys. Lett.* **82**, 940 (2003).
- ⁷S. Denis, L. Dusoulier, M. Dirickx, Ph. Vanderbemden, R. Cloots, M. Ausloos, and B. Vanderheyden, *Supercond. Sci. Technol.* **20**, 192 (2007).
- ⁸C. P. Bean, *Rev. Mod. Phys.* **36**, 31 (1964).
- ⁹E. H. Brandt, *Phys. Rev. B* **58**, 6506 (1998).
- ¹⁰A. Sanchez and C. Navau, *Phys. Rev. B* **64**, 214506 (2001).
- ¹¹S. Denis, M. Dirickx, Ph. Vanderbemden, M. Ausloos, and B. Vanderheyden, *Supercond. Sci. Technol.* **20**, 418 (2007).
- ¹²J.-F. Fagnard, M. Dirickx, M. Ausloos, G. Lousberg, B. Vanderheyden, and Ph. Vanderbemden, *Supercond. Sci. Technol.* **22**, 105002 (2009).
- ¹³C. Navau, N. Del-Valle, and A. Sanchez, *IEEE Trans. Appl. Supercond.* **23**, 8201023 (2013).
- ¹⁴M. Tinkham, *Introduction to Superconductivity*, 2nd ed. (Dover, 2004).
- ¹⁵T. Van Duzer and C. W. Turner, *Principles of Superconductive Devices and Circuits* (Edward Arnold, 1998).
- ¹⁶V. A. Schweigert, F. M. Peeters, and P. Singha Deo, *Phys. Rev. Lett.* **81**, 2783 (1998).
- ¹⁷B. Xu, M. V. Milosevic, and F. M. Peeters, *Phys. Rev. B* **77**, 144509 (2008).
- ¹⁸M. V. Milosevic and R. Geurts, *Physica C* **470**, 791 (2010).
- ¹⁹R. Geurts, M. V. Milosevic, and F. M. Peeters, *Phys. Rev. B* **81**, 214514 (2010).
- ²⁰M. Tomsic, M. Rindfleisch, J. Yue, K. McFadden, J. Phillips, M. D. Sumption, M. Bhatia, S. Bohnenstiehl, and E. W. Collings, *Int. J. Appl. Ceram. Technol.* **4**, 250 (2007).
- ²¹L. Gozzelino, F. Laviano, D. Botta, A. Chiodoni, R. Gerbaldo, G. Ghigo, E. Mezzetti, G. Giunchi, S. Ceresara, and G. Ripamonti, *Philos. Mag. B* **82**, 1 (2002).
- ²²P. Mikheenko, V. V. Yurchenko, and T. H. Johansen, *Supercond. Sci. Technol.* **25**, 045009 (2012).

- ²³J. Noudem, P. Bernstein, and Y. Thimont, French patent FR 1255988 (2012).
- ²⁴L. Gozzelino, B. Minetti, R. Gerbaldo, G. Ghigo, F. Laviano, G. Lopardo, C. Plapcianu, and A. Agostino, *J. Supercond. Novel Magn.* **24**, 307 (2011).
- ²⁵See <http://www.comsol.com/> for “Comsol Multiphysics modeling and simulation software.”
- ²⁶F. Manzano, A. Carrington, N. E. Hussey, S. Lee, A. Yamamoto, and S. Tajima, *Phys. Rev. Lett.* **88**, 047002 (2002).
- ²⁷FCT System GmbH, HP D25, Rauenstein, Germany.
- ²⁸H. C. Starck, GmbH, Goslar, Germany.
- ²⁹E. Altshuler and T. H. Johansen, *Rev. Mod. Phys.* **76**, 471 (2004).
- ³⁰G. Ghigo, R. Gerbaldo, L. Gozzelino, F. Laviano, G. Lopardo, E. Monticone, C. Portesi, and E. Mezzetti, *Appl. Phys. Lett.* **94**, 052505 (2009).
- ³¹L. Gozzelino, B. Minetti, R. Gerbaldo, G. Ghigo, F. Laviano, A. Agostino, and E. Mezzetti, *IEEE Trans. Appl. Supercond.* **21**, 3146 (2011).